Supplement of Aerosol Research, 2, 107–122, 2024
https://doi.org/10.5194/ar-2-107-2024-supplement

AEROSOL Research
Open Access

Supplement of

Assessment of light-absorbing carbonaceous aerosol origins and properties at the ATOLL site in northern France

Alejandra Velazquez-Garcia et al.

Correspondence to: Alejandra Velazquez-Garcia (ale-vg13@hotmail.com) and Joel F. de Brito (joel.brito@imt-nord-europe.fr)

Sector-specific grid maps for black carbon emissions

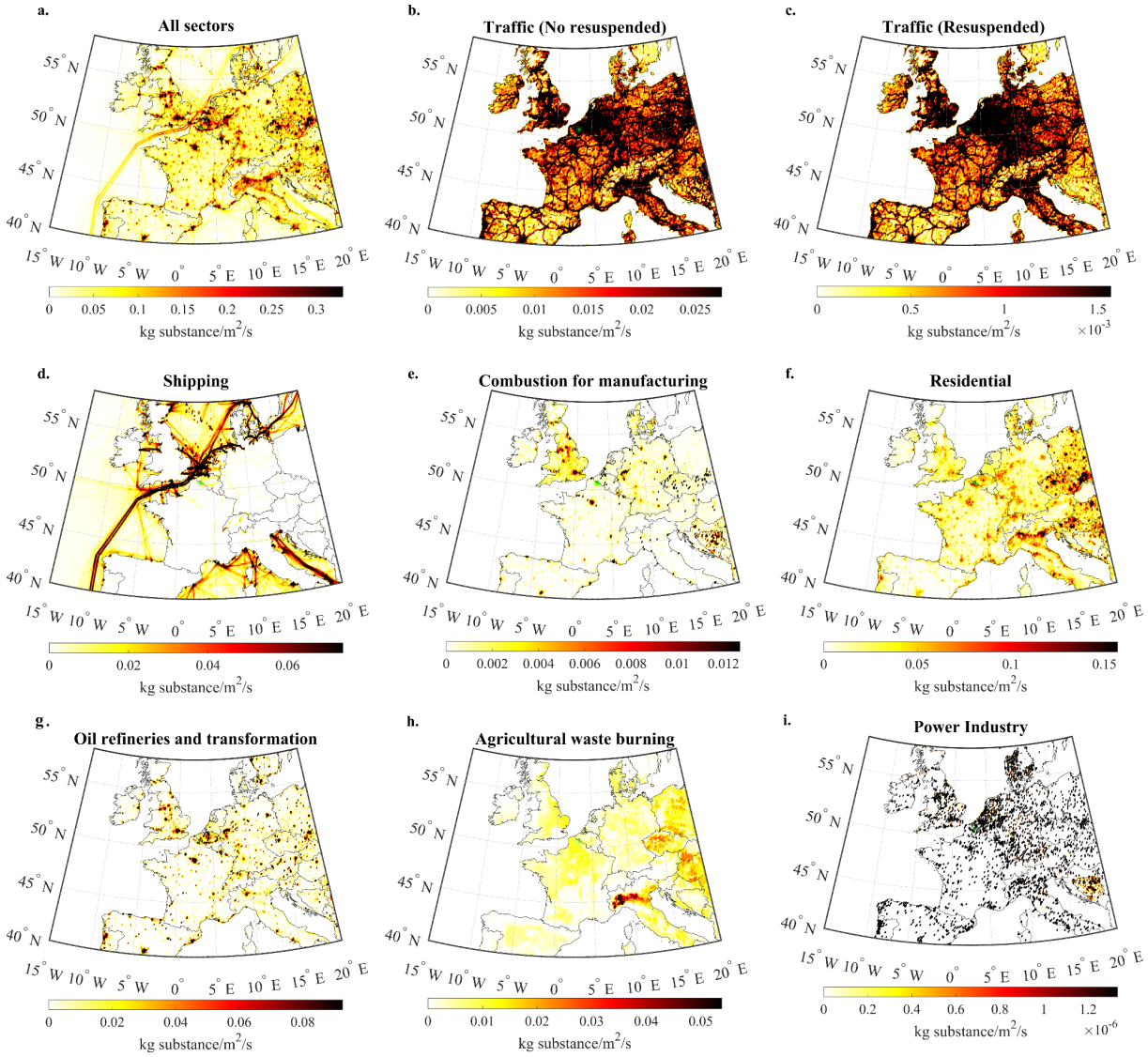

Figure S1: Sector-specific grid maps in kg of Black Carbon/m²/s (5th - 95th percentile) from EDGAR v6.1 (https://edgar.jrc.ec.europa.eu/index.php/dataset_ap61). Note the range of the color scale varies for each map. (a) All sectors combined. (b) Tail-pipe traffic emissions. (c) Traffic resuspension. (d) Shipping emissions, including on rivers and canals. (e) Industry-manufacturing, generation of electricity and heat for own usage. (f) Residential sector, generation of heat (biomass or liquid fuel). (g) Oil refineries and transformation – refining petroleum products and production of charcoal. (h) Agricultural waste burning. (i) Power industry, producers of electricity generation, heat and power generation.

Air mass arrival sector criteria

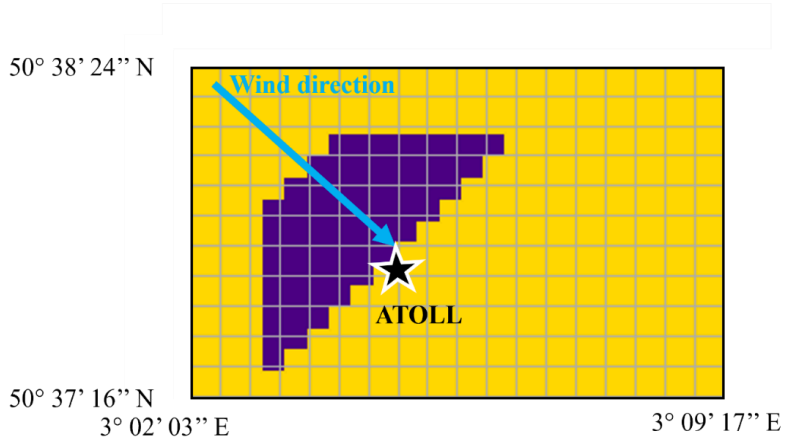

Figure S2: Contribution of the vicinity (<40km, indigo color) to the ATOLL platform according to the incoming air mass trajectory. The squares represent the EDGAR spatial resolution (0.1° x 0.1°) and the arrow is the arrival sector. One can see that, the indigo color area accounts for the local contribution ("Lille") whereas the yellow color area does not.

Minimum contribution of the total integrated BC for individual back trajectories

Table S1: Tested percentages serving as benchmarks to establish the minimum level of integrated total black carbon contribution for individual back trajectories (BT).

Country or, Sector	Minimum contribution	# of BTs
France	10%	368
Belgium		155
UK		82
Germany		77
Traffic		994
Residential		642
Shipping		850
Industry		765
France	30%	140
Belgium		27
UK		5
Germany		23
Traffic		482
Residential		151
Shipping		496
Industry		10
France	50%	51
Belgium		2
UK		0
Germany		3
Traffic		38
Residential		6
Shipping		241
Industry		0

Black carbon baseline

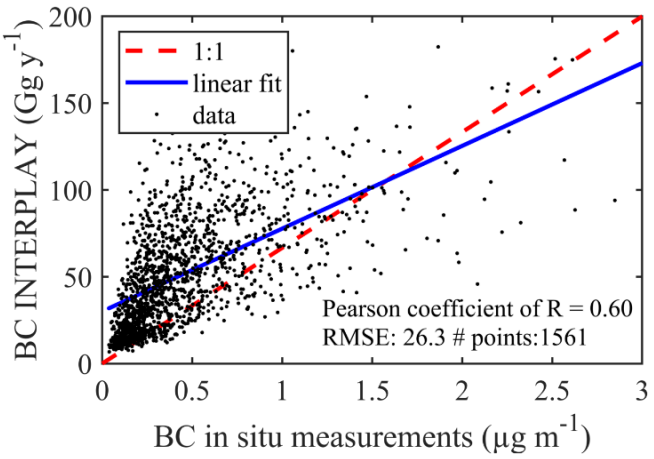

Figure S3: Linear correlation between the INTERPLAY approach and in situ BC observations within an hourly average integrated into a baseline of 12 hrs.

HYSPLIT backward trajectory ensemble analysis

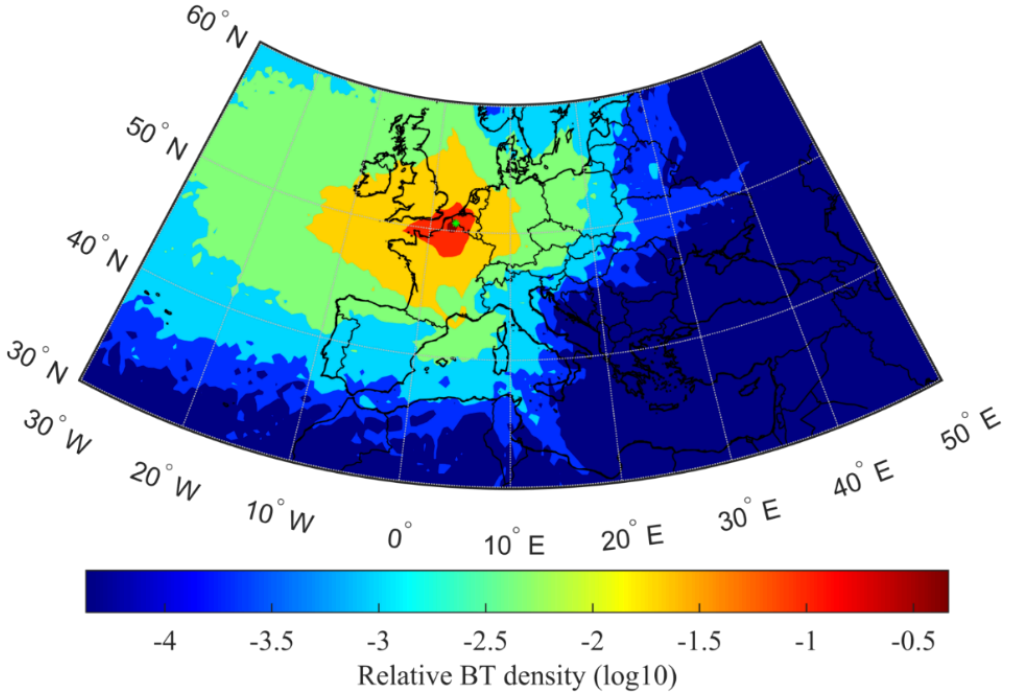

Figure S4: HYSPLIT backward trajectory (BT) ensembles showing the large-scale trade wind circulation influence at the ATOLL platform by means of air mass residence time maps. The BT ensembles comprise all 26 808 individual 3D BTs, spanning a multi-year period from Dec 2016 until Dec 2019. For the 72h BT, only 19% of points were found to be above the PBL height, with a fairly small effect.

INTERPLAY results

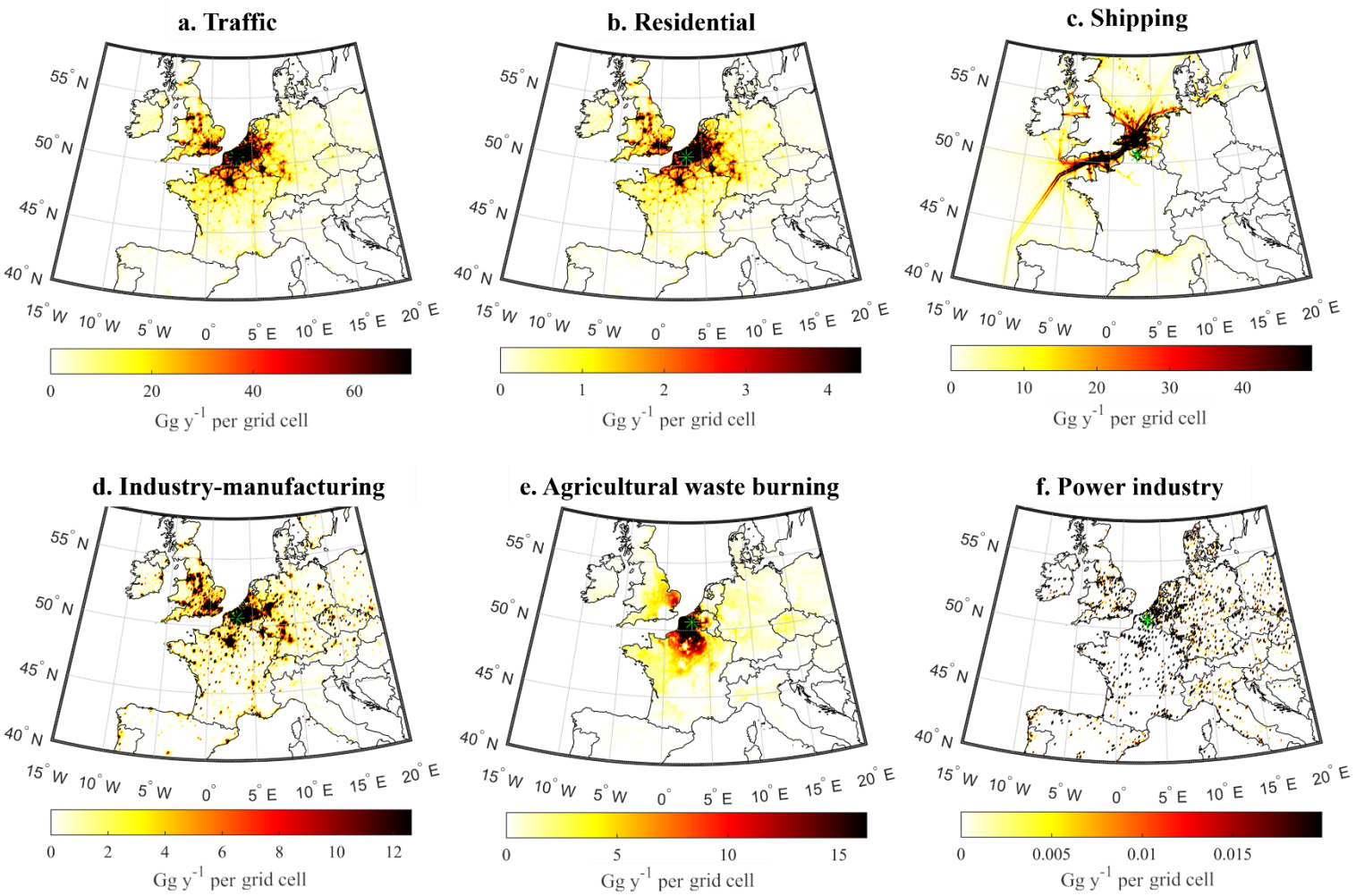

Figure S5: Accumulated contribution of BC to ATOLL in Gg y^{-1} per grid cell for (a) traffic, (b) residential sector, (c) shipping emissions, (d) industry-manufacturing counting oil refineries and transformation as well as combustion for manufacturing, (e) agricultural waste burning, (f) power industry over the period Dec 2016 – Dec 2019. The term "others" refers to oceans, channels, and other regions in Europe.

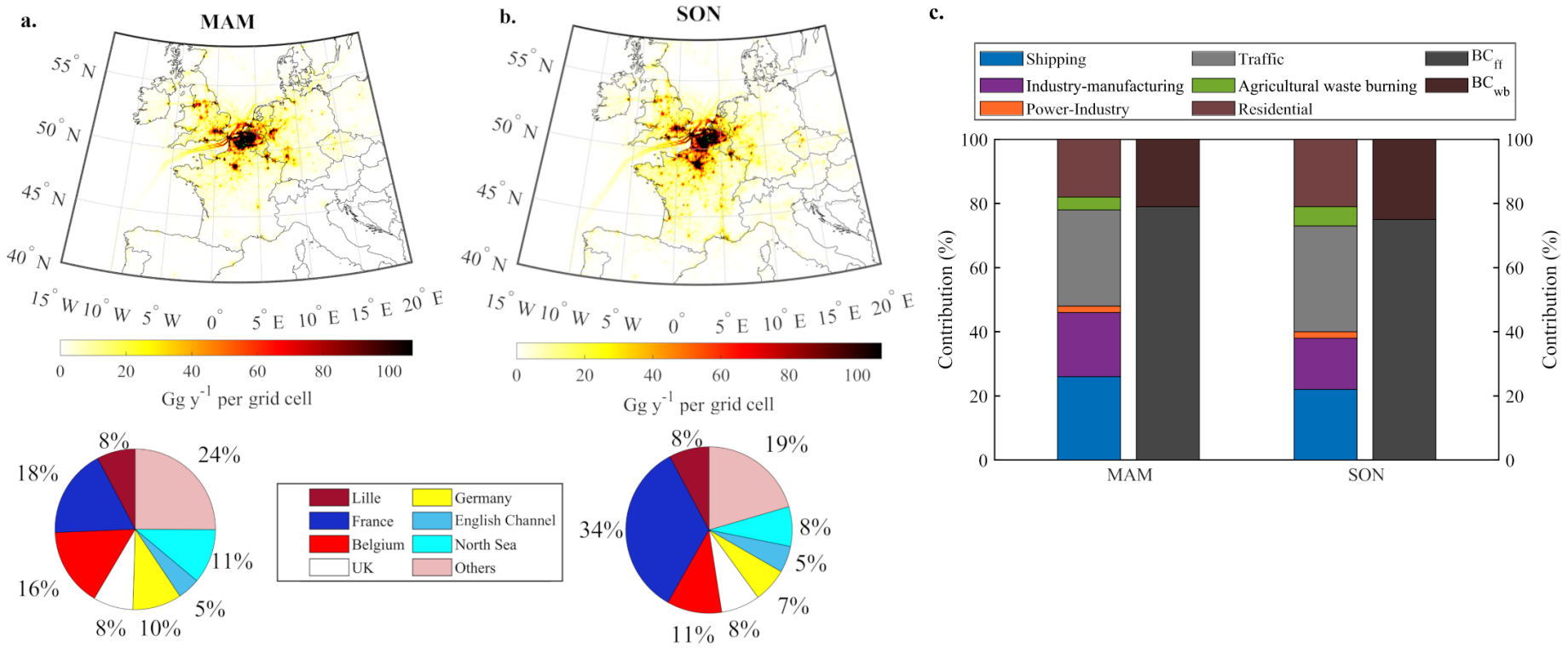

Figure S6: Spatial contribution of BC to ATOLL in Gg y^{-1} per grid cell and its relative contribution by region/country for spring (a) and fall (b) note that France does not include Lille's contribution; c) sectorial distributions according to INTERPLAY and in-situ via the aethalometer model. Results over the period Dec 2016 – Dec 2019.

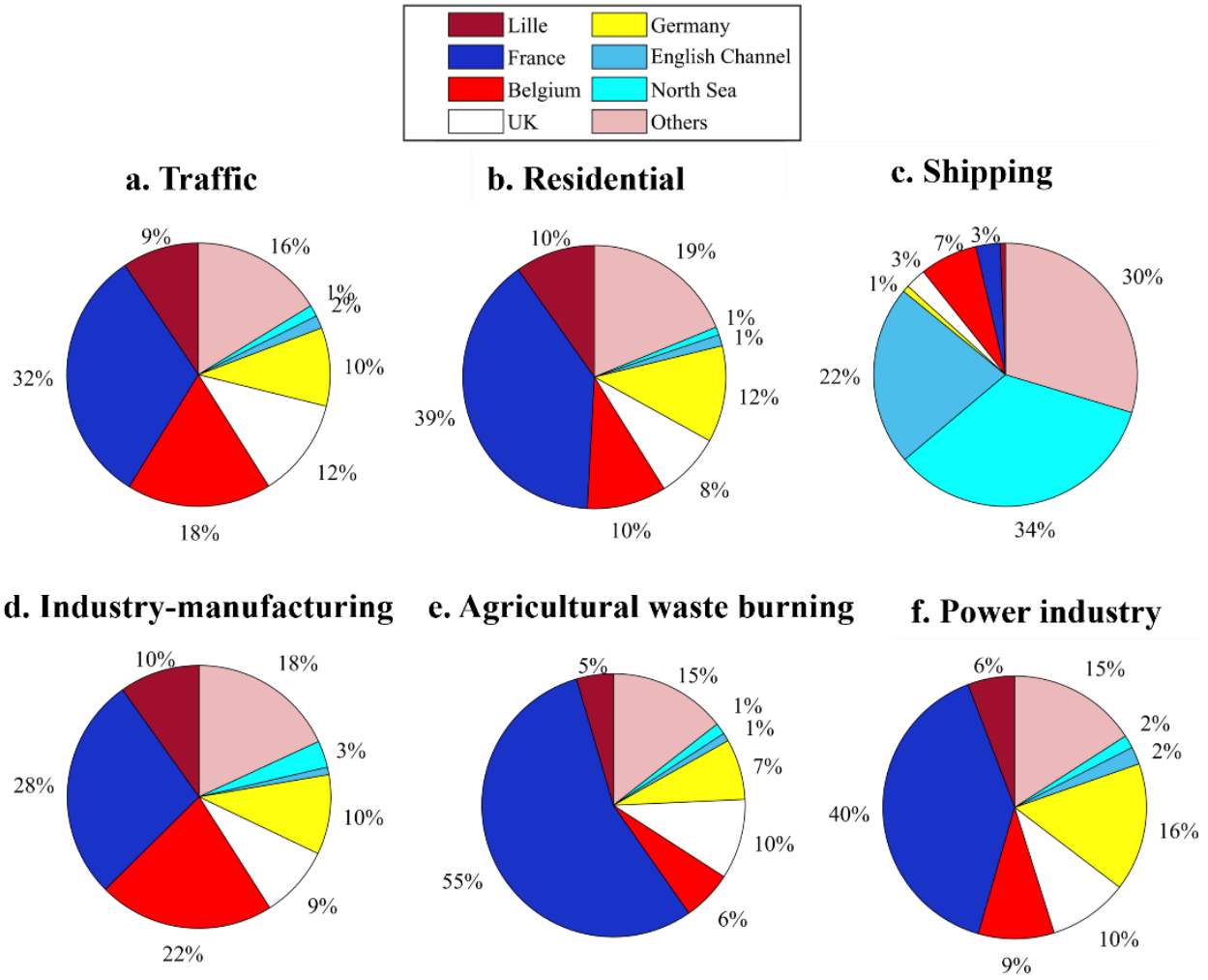

Figure S7: Relative distribution of BC to ATOLL by geographical origin for (a) traffic, (b) residential sector, (c) shipping emissions, (d) industry-manufacturing including oil refineries and transformation as well as combustion for manufacturing, (e) agricultural waste burning, (f) power industry over the period Dec 2016 – Dec 2019. The term "others" refers to oceans, channels, and other regions in Europe.

Light-absorbing carbonaceous aerosol apportionment

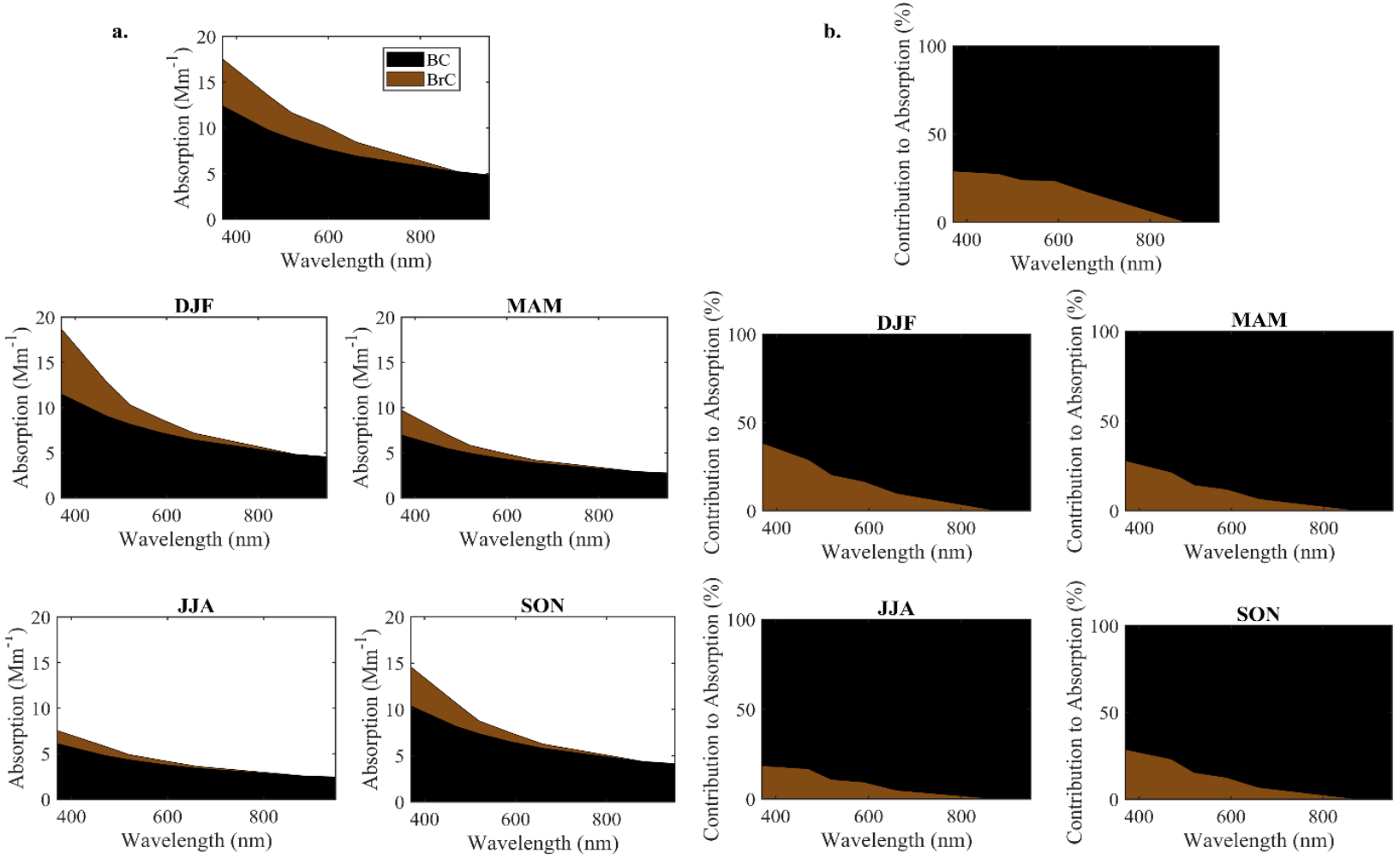

Figure S8: BC and BrC apportionment at the ATOLL site. a. Site average (in Mm^{-1}) and b. contribution to absorption (in percentage) for all data (top) and per season (bottom).

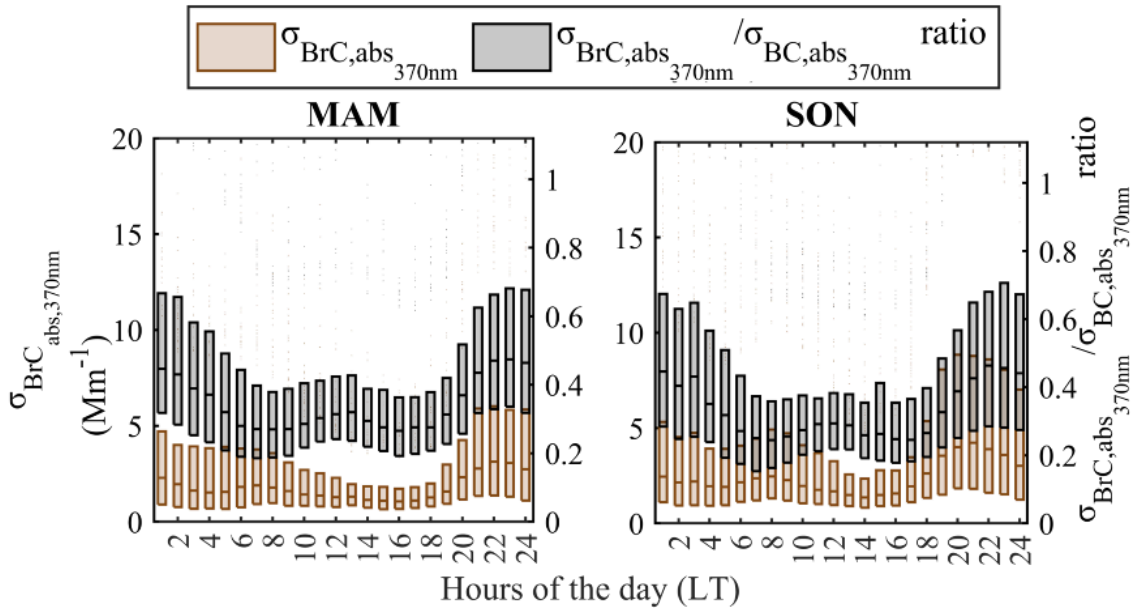

Figure S9: Diel cycles of BrC absorption (in Mm^{-1}) (left y-axis) and BrC fraction (right y-axis) calculated at 370 nm at the ATOLL platform. The line is the median, whereas the box shows the interquartile range.

Multiple Linear Regression of BrC

BrC lifetime was studied using Multiple Linear Regression (MLR). Aiming to reduce multicollinearity in the MLR, we selected the dependent variables following the two main sources of light-absorbing carbonaceous aerosols reported for suburban and urban European sites (Chen et al. 2022, Savadkoohi et al. 2023). Additionally, a well-established BrC component is associated with wood burning and BC with fossil fuel via the Aethalometer model (Sandradewi et al. 2008). Thus, traffic and residential have been selected. Including further components as predictors in the MLR would increase the variance in the regression coefficients, making them unstable and complex to interpret (Shrestha, 2020).

Figures S10 and S11 show the results of the test regarding the time from emission considering 6, 12, 24, and 36 hours. Overall, the fresh BC from the residential sector dominates the relative contribution to the BrC absorption at 470 nm (between 51 and 82%) whereas the contribution to the mass is largely governed by the aged aerosols for low times from emissions (76% at 6 hours) but decreases with increasing time from emissions (30% at 36 hours), suggesting a decrease in the BrC component.

These results are consistent with literature data. For instance, Forrister et al. (2015) and (Selimovic et al., 2019)) observed a substantial decay in aerosol UV light absorption in biomass-burning plumes, corresponding to a 9 to 15-hour half-life. (Saleh, 2020)) compared studies performed in laboratory conditions with atmospheric observations, and highlighted that the latter reported longer BrC absorption lifetimes (~1 day) (Forrister et al., 2015; Wang et al., 2019; Wong et al., 2019) than laboratory experiments (hours).

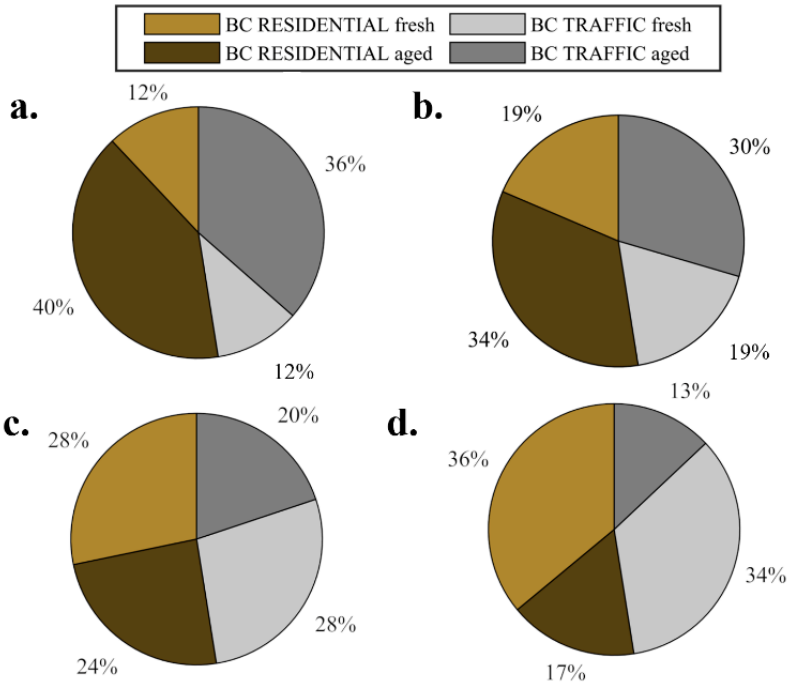

Figure S10: Relative contributions to the mass of different BC sources (residential, traffic) depending on the time from emission: x = 6 hours (a), x = 12 hours (b), x = 24 hours (c), and x = 36 hours (d). BC emitted from less than x hours is labelled as "fresh", while BC emitted from more than x hours is termed "aged".

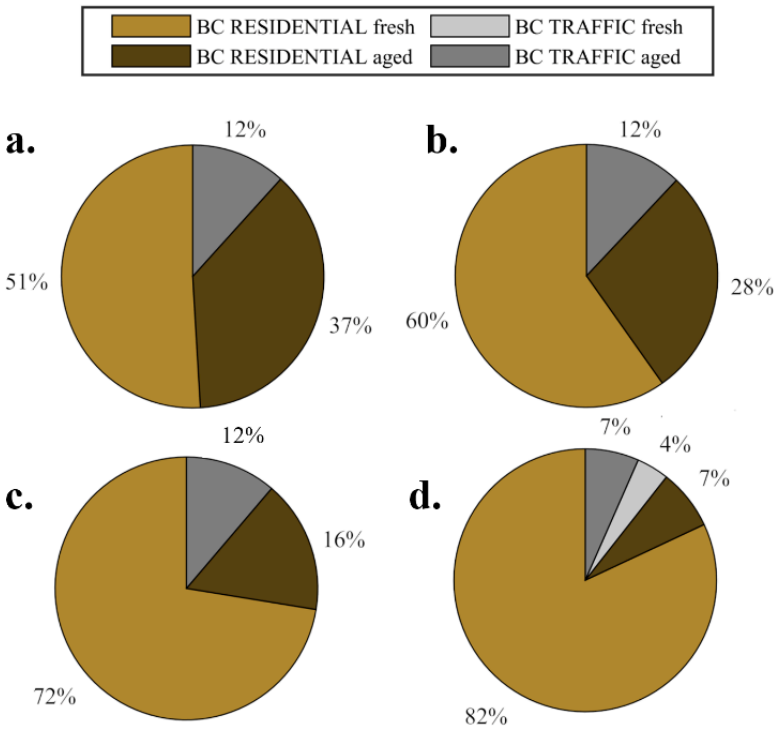

Figure S11: Relative contributions to light absorption calculated at 470 nm explained by the BC sources (residential, traffic) depending on the time from emission: x = 6 hours (a), x = 12 hours (b), x = 24 hours (c), and x = 36 hours (d). BC emitted from less than x hours is labelled as "fresh", while BC emitted from more than x hours is termed "aged".

Table S2 reports the MAEs of two sources (traffic and residential) distinguished between time of emission. The fresh ones correspond to a time from emission of less than 24 hours, whereas aged ones were emitted more than 24 hours ago. The four variables were included in the linear regression to retrieve their respective MAE at 470 nm. MAE are key parameters used to estimate aerosol radiation impact from chemical properties and within models. (Seinfeld and Pandis, 2012).

Table S2: Mass Absorption Efficiency (MAE) retrieved with a Multiple Linear Regression for the BC INTERPLAY components considering a threshold for time from emission at 24 hours (case b in Figures S11 and S12).

Sources	MAE at 470 nm (m^2 g^{-1})
Residential fresh	1.14
Residential aged	0.03
Traffic fresh	-
Traffic aged	0.02

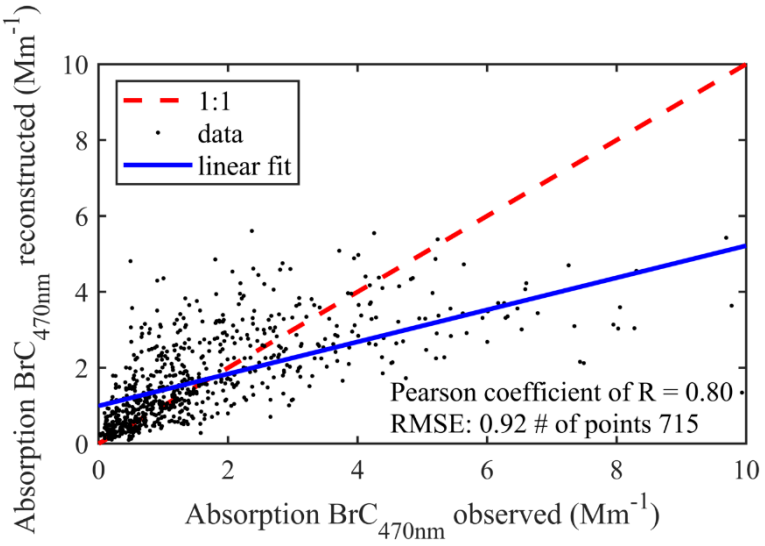

Figure S12: Observed vs modeled BrC absorption at 470 nm using MLR analysis with four classes (fresh or aged emissions from traffic or residential sectors from the INTERPLAY approach).

INTERPLAY main code

Variables description

time_BT: arrival time of HYSPLIT back trajectories.
time_AE33: time stamp of AE33 in-situ observations.
idx_flag: flagging for local contamination (1) or not (0).
EBC: Matrix of EBC values (7 wavelengths) from AE33.
lon, lat: position from HYSPLIT. The first position is the arrival point (i.e. ATOLL).
lon_inv, lat_inv: grid position from EDGAR inventory.
BC_GP: integrated BC along the backtrajectory.

```
for i=1:max(size(time_BT))

    idx=find(time_AE33>=time_BT(i)&time_AE33<time_BT(i)+1./24&idx_flag==0);
    m0_str=num2str(month(time_BT(i)));

    if min(size(idx))>0
        EBC_corr(i,:)=nanmean(EBC(idx,:));

        for j=1:size(lat,1)
            idx_lon=find(lon(j,i)>=(lon_inv-size_rec./2)&lon(j,i)<=(lon_inv+size_rec./2));
            idx_lat=find(lat(j,i)>=(lat_inv-size_rec./2)&lat(j,i)<=(lat_inv+size_rec./2));
            dist_point(j,i)=pos2dist(lat(1,1),lon(1,1),lat(j,i),lon(j,i),2);

            dummy_idx=ones(size(idx_lon,1),size(idx_lat,1));
            if dist_point(j,i)<40 %this is the distance where the rectangle can include downtown lille
                [X,Y] = meshgrid(lon_inv(idx_lon),lat_inv(idx_lat));
                lat_circle=lat(1,1)+2.*sind(Li_vector(i)+d_Sec);
                lon_circle=lon(1,1)+2.*cosd(Li_vector(i)+d_Sec);%200km selected
                [dummy_idx,~]=inpolygon(X,Y,[lon(1,1) lon_circle lon(1,1)],[lat(1,1) lat_circle lat(1,1)]);%0.5
                dummy_idx=dummy_idx';
            end
            eval(['BC_GP(j,i)=sum(sum(BC_sum_',m0_str,'(idx_lon,idx_lat).*dummy_idx));'])
            count_filter(j,i)=nansum(nansum(dummy_idx))./(size(dummy_idx,1).*size(dummy_idx,2));

            for k=1:max(size(sector))
                eval(['BC_GP_',sector{k},'(j,i)=sum(sum(BC_',sector{k},'_',m0_str,'(idx_lon,idx_lat).*dummy_idx));'])
            end

        end
    else
        EBC_corr(i,:)=ones(7,1).*NaN;
        BC_GP(1:size(lat,1),i)=NaN;
        count_filter(1:size(lat,1),i)=NaN;

        for k=1:max(size(sector))
            eval(['BC_GP_',sector{k},'(1:size(lat,1),i)=NaN;'])
        end

    end
end

%% ------ Filter rain-------- %%
idx=intersect(idx,find(nanmax(rain)<1));
size(idx)
LM=fitlm(EBC_corr(idx,6),nansum(BC_GP(:,idx)))
nanmean(count_filter(:,1))
```

References

Chen, Gang et al. 2022. “European Aerosol Phenomenology − 8: Harmonised Source Apportionment of Organic Aerosol Using 22 Year-Long ACSM/AMS Datasets.” *Environment International* 166: 107325.

Forrister, H., Liu, J., Scheuer, E., Dibb, J., Ziemba, L., Thornhill, K. L., Anderson, B., Diskin, G., Perring, A. E., Schwarz, J. P., Campuzano-Jost, P., Day, D. A., Palm, B. B., Jimenez, J. L., Nenes, A., and Weber, R. J.: Evolution of brown carbon in wildfire plumes, Geophys. Res. Lett., 42, 4623–4630, https://doi.org/10.1002/2015GL063897, 2015.

Saleh, R.: From Measurements to Models: Toward Accurate Representation of Brown Carbon in Climate Calculations, Curr. Pollut. Rep., 6, 90–104, https://doi.org/10.1007/s40726-020-00139-3, 2020.

Selimovic, V., Yokelson, R. J., McMeeking, G. R., and Coefield, S.: In situ measurements of trace gases, PM, and aerosol optical properties during the 2017 NW US wildfire smoke event, Atmospheric Chem. Phys., 19, 3905–3926, https://doi.org/10.5194/acp-19-3905-2019, 2019.

Shrestha, N.: Detecting Multicollinearity in Regression Analysis, Am. J. Appl. Math. Stat., 8, 39–42, https://doi.org/10.12691/ajams-8-2-1, 2020.

Wang, Q., Ye, J., Wang, Y., Zhang, T., Ran, W., Wu, Y., Tian, J., Li, L., Zhou, Y., Hang Ho, S. S., Dang, B., Zhang, Q., Zhang, R., Chen, Y., Zhu, C., and Cao, J.: Wintertime Optical Properties of Primary and Secondary Brown Carbon at a Regional Site in the North China Plain, Environ. Sci. Technol., 53, 12389–12397, https://doi.org/10.1021/acs.est.9b03406, 2019.

Wong, J. P. S., Tsagkaraki, M., Tsiodra, I., Mihalopoulos, N., Violaki, K., Kanakidou, M., Sciare, J., Nenes, A., and Weber, R. J.: Atmospheric evolution of molecular-weight-separated brown carbon from biomass burning, Atmospheric Chem. Phys., 19, 7319–7334, https://doi.org/10.5194/acp-19-7319-2019, 2019.